Direct visualization of first-order magnetic transition in $La_{5/8-y}Pr_yCa_{3/8}MnO_3$ ($y = 0.45$) thin films

R. Rawat, Pallavi Kushwaha, Dileep K. Mishra, and V. G. Sathe
UGC-DAE Consortium for Scientific Research, University Campus, Khandwa Road, Indore-452001, India
(Received 30 July 2012; published 13 February 2013)

First-order antiferromagnetic insulating (AFI)-ferromagnetic metallic (FMM) transition as a function of temperature and magnetic field has been imaged using magnetic force microscopy (MFM) in $La_{5/8-y}Pr_yCa_{3/8}MnO_3$ ($y = 0.45$) thin film grown on $NdGaO_3$ substrate. These images, showing AFI to FMM transformation during in-field cooling and reverse transformation during warming of the same region, cannot be described solely in terms of the broad first-order transition due to quench disorder. Growth morphology of the FMM phase is observed to be path dependent as larger size FMM regions (but with smaller net fraction) are observed for isothermal field induced transition when compared to isofield thermal transition. This is shown to be a consequence of the glasslike arrested AFI state even at ≈100 K. Apparent variable range hopping like transport near T_{MI} during cooling is shown to be a consequence of growth of the FMM phase in an AFI matrix.

DOI: 10.1103/PhysRevB.87.064412 PACS number(s): 75.30.Kz, 68.37.Rt, 72.15.Gd, 75.47.Gk

Broad first-order phase transition (FOPT) due to quench disorder has been a subject matter of investigation in diverse materials, particularly in the correlated electron systems. In manganites, phase coexistence associated with FOPT is believed to be one of the main ingredients for observed colossal magnetoresistance (CMR).[1] In these systems, the electronically and magnetically contrasting antiferromagnetic insulator (AFI) and ferromagnetic metallic (FMM) phases are found to coexist over a wide range of temperature and magnetic field.[2] There have been several microscopic studies to probe the length scale of phase separation, particularly in $La_{5/8-y}Pr_yCa_{3/8}MnO_3$ (LPCMO) where phase coexistence is observed over a several micrometer length scale along with the observation of glasslike magnetic states at low temperatures.[3–10] Direct visual evidence of percolative metal-insulator (MI) transition was given by Zhang *et al.*[7] in $La_{0.33}Pr_{0.34}Ca_{0.33}MnO_3$ thin film using magnetic force microscopy (MFM). Spectroscopic studies for $y = 3/8$ also showed phase separation on the length scale of several micrometer.[10] On the other hand, transmission electron microscopic results for $y = 0.275$–0.3 were interpreted in terms of the coexistence of FMM and AFI states on the length scale of nanometers to a few micrometers.[11] Recent studies by Burkhardt *et al.*[9] have shown that the correlation length of AFI is less than 150 nm, whereas FMM regions grow up to several micrometers. Besides different length scales of the observed phase separation on different compositions by different techniques, microscopic studies on higher y with predominantly AFI state are rare.

Here, we investigate the nucleation and growth of the FMM/AFI phase during cooling, warming, and isothermal field cycling across the MI transition in LPCMO ($y = 0.45$) thin film (≈150 nm thick) deposited on the $NdGaO_3$ (NGO) substrate. In our earlier study of this LPCMO thin film, we showed that the ground state is FMM and the AFI state is a glasslike magnetic state that is a manifestation of arrested kinetics.[12] Here, we image the AFI-FMM transformation of the same region of the sample over a wide temperature range during cooling and warming using in-field MFM. These measurements provide direct visual evidence that nucleation and growth of the FMM phase across the AFI-FMM transition cannot be represented by broad first-order transition due to quench disorder. It is also observed that the isothermal field induced transition results in different growth morphology due to the kinetically arrested AFI state even at 100 K during zero field cooling.

Sample preparation and characterization of the LPCMO/NGO film are given in Ref. 12. MFM from NanoMagnetics Instruments, UK, along with a superconducting magnet system from American Magnetics, USA, is used for magnetic imaging. All the MFM scans presented in this manuscript are carried out with a scan speed of 2 μm/sec using a Co coated n-Si cantilever (PP-MFPR from Nanosensor; resonance frequency ≈67 kHz) and with an applied magnetic field direction perpendicular to the film plane. Topography is measured during the forward scan and magnetic contrast (or phase shift) is measured during the reverse scan in which a cantilever follows the topography measured in the forward scan with a 50 nm liftoff.

Figure 1(a) shows the resistivity during cooling and subsequent warming in the presence of various magnetic fields. Zero field resistivity does not show any transition or thermal hysteresis, whereas cooling under 1 T magnetic field results in MI transition around 80 K followed by approximately two orders of change in ρ value. At higher fields ($\geqslant$2 T), MI transition temperature (T_{MI}) shifts to higher temperature with decreasing hysteresis. In addition, we observed different transport mechanisms in different temperature regions above T_{MI}, which are highlighted in Figs. 1(b)–1(c) for 1 T applied magnetic field. Resistivity follows activated behavior above ≈140 K [Fig. 1(b)] and deviates from it at lower temperatures. In the temperature range ≈140 K to T_{MI} linear $\log(\rho)$ versus $T^{-1/4}$ behavior is observed [Fig. 1(c)], which is generally expected for variable range hopping. On the other hand, MFM results (that follows) show that the deviation from $\ln(\rho)$ versus T^{-1} below 140 K is a consequence of the phase coexistence rather than the change in transport mechanism.

The MFM images taken in the presence of 1 T magnetic field are shown in Fig. 2 during cooling (125–60 K) and in Fig. 3 for subsequent warming (60–150 K). By tracking topographic features, the same region (within 10% accuracy) is scanned at all the temperatures to study the nucleation

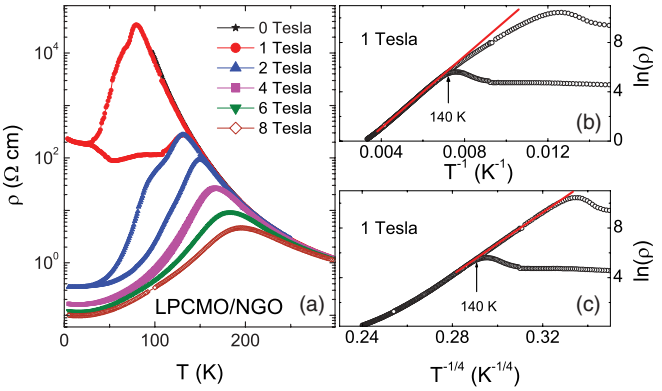

FIG. 1. (Color online) (a) Resistivity (ρ) as a function of temperature under various magnetic field depicting MI transition for $\geqslant$1 T for LPCMO film on NGO substrate. (b) ln(ρ) vs T^{-1} and (c) ln(ρ) vs $T^{-1/4}$ for cooling and warming under 1 T.

and growth process across the MI transition. The 125 K MFM image shows well separated FMM nuclei (dark color). The average size/aspect ratio of the FMM nuclei increases from 230 nm/1.5 to 1300 nm/1.8 with lowering temperature from 125 to 80 K. Percolation sets in around 80 K, which is consistent with the 1 T ρ-T data shown in Fig. 1. Few percolative paths are highlighted in the 80 and 90 K images by white lines. In the light of these measurements, it is evident that the apparent $T^{-1/4}$ behavior or smaller ρ than that expected from activated behavior near T_{MI} [Fig. 1(b)] is a result of reduced AFI phase fraction.

MFM images during warming (Fig. 3) remained unchanged up to 125 K, as can be seen from a magnetic contrast for this image that is identical to the 60 K image (shown in Fig. 2). Around 130 K reverse transformation sets in and AFI regions grow at the expense of FMM regions. Around 140 K, percolation in FMM clusters break down and the average size/aspect ratio of the FMM clusters reduces from 1315 nm/1.8 to 230 nm/1.5 upon warming from 140 to 150 K. In short, these MFM images show that the FMM phase coexists with the AFI phase well above T_{MI}, and percolation temperature both during cooling and warming matches with the T_{MI} obtained from the ρ-T measurement.

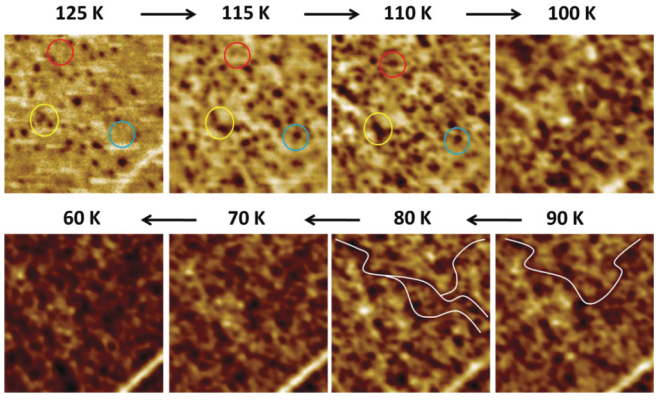

FIG. 2. (Color online) MFM images (5 μm $\times$ 5 μm) showing AFI (light) to FMM (dark) transition during 1 T field cooling (applied isothermally at 125 K). The scale for 125 K to 60 K images are 8, 15, 19, 30, 44, 63, 63, and 55 degrees, respectively.

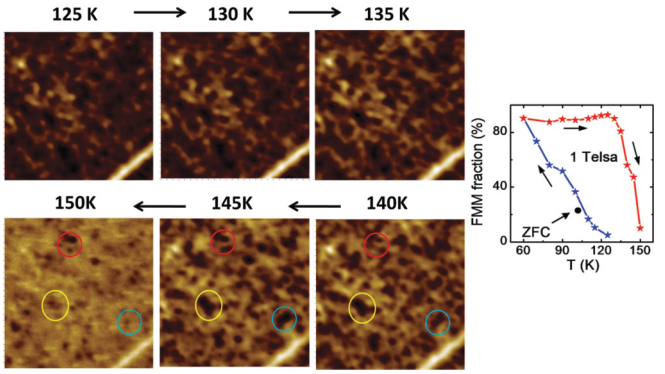

FIG. 3. (Color online) FMM (dark) to AFI (light) transition during warming under 1 T magnetic field after field cooling to 60 K. The scale for images (5 μm $\times$ 5 μm) from 125 K to 150 K are 40, 39, 30, 21, 9, and 4 degrees, respectively. Right panel shows FMM phase fraction estimated from MFM images collected during 1 T field cooling (blue star) and subsequent warming (red star), and at 102 K/1 T after zero field cooling (black circle).

The right panel of Fig. 3 shows the variation of FMM phase fraction (estimated from MFM images) during 1 T cooling and subsequent warming. Regions with more (less) than 50% of the maximum phase shift in the respective image are considered FMM (AFM) regions. During cooling, the FMM phase fraction increases continuously from 125 K to the lowest temperature of MFM measurement, i.e., 60 K. On the other hand this phase fraction remains nearly constant during warming up to 125 K, above which it decreases rapidly, and the system becomes almost AFI by 150 K. This behavior is typical of the bulk magnetization (M) behavior observed for LPCMO systems where continuous change in M across the AFI-FMM transition is generally associated with a broad first-order transition due to quench disorder. In such transitions, disorder gives rise to spatial distribution of transition temperature on the length scale of correlation length.[13,14] In this picture, if the observed transition temperature during cooling (T^{*}_{MI}) for a given region is lower, then it should also have lower transformation temperature during warming (T^{**}_{MI}), i.e., for regions A and B if $T^{*}_{MI}(A) < T^{*}_{MI}(B)$ then $T^{**}_{MI}(A) < T^{**}_{MI}(B)$. This has been shown on a mesoscopic length scale in Ru doped $CeFe_2$ for an isothermal field induced transition using scanning hall probe studies.[15] To the best of our knowledge there are no scanning probe studies where transformation of the same region is tracked during cooling and warming. This is mainly due to the difficulty in retaining the same region on such a small length scale over a large temperature range, as well as the time required for measurements. In the present study, we are able to retain the same area of the sample at all the temperatures within 10% accuracy.

In order to highlight the transformation process, three regions are marked by color circles in Figs. 2 and 3. During cooling the FMM phase appears at lower temperature in the blue (bottom right) circled region than the yellow (bottom left) circled region. Upon warming also, the FMM region disappears at lower temperature in the blue circled region, therefore following the condition: if $T^{*}_{MI}(A) < T^{*}_{MI}(B)$ then $T^{**}_{MI}(A) < T^{**}_{MI}(B)$. On the other hand, the region marked by a red circle (top) behaves differently. It shows the presence

TABLE I. Temperature variation of yellow, red, and blue like FMM regions during cooling (125–110 K) and warming (140–150 K) in terms of area percentile/no. of regions.

Temperature	125 K	115 K	110 K	140 K	145 K	150 K
Yellow	5/15	5/13	6/12	6/12	22/11	5/11
Blue		3/7	4/7	10/5	1/2	
Red		4/7	7/10	26/10	23/11	5/11

of the FMM phase at 150 K during warming, whereas no such FMM phase is seen at the 125 K image during cooling. Thus, the region highlighted by the top circle (red) shows transition at lower temperature (see the 115 K image) during cooling compared to the other two regions (yellow and green), whereas reverse transformation for the top circle is observed at higher temperature. Table I summarizes temperature variation of the red and blue like area in terms of percentile area/no. of regions with respect to the 125 K (yellow regions) image. This analysis shows that chemical inhomogeneity is not entirely responsible for phase separation. Such a behavior may arise due to distribution in strain across film thickness. In fact different surface, interface, and bulk behavior is reported in similar systems.[16,17] Variation in strain across film thickness can lead to MFM images that show FMM nuclei at higher temperature (125 K) but its absence at lower temperature (115 and 110 K) during cooling as shown in Fig. 2. The analysis of these images showed that this is due to growth of the higher magnetization FMM phase in the nearby region. This suggests that the FMM and AFI phase could be coexisting across the film thickness, which results in different magnetization (and hence phase shift) for two FMM regions.

It is interesting to compare our results with the MFM measurements of Zhang *et al.*[7] on $La_{0.33}Pr_{0.34}Ca_{0.33}MnO_3$ thin film. They observed growth of the FMM phase and percolation well below T_{MI}. On the other hand our MFM study show that nucleation starts with submicrometer-size nuclei well above T_{MI} and percolation sets in around this temperature. This difference can be explained by considering the different measurement conditions used in the two experiments. In the absence of magnetic field (which is the case in Ref. 7) randomly oriented domains were visualized with magnetization direction predominantly oriented along the film plane. This results in weaker (in magnitude) contrast as well as larger (in space) FMM regions. The other interesting feature in MFM images of Zhang *et al.*[7] is apparently weaker contrast and smaller FMM phase during warming when compared to cooling. This was attributed to different measurement protocol for the cooling and warming cycle even though the measurement parameters were identical. Earlier studies have shown that the state of these systems depends on the path or history of the sample.[3–5,8,12,14] At low temperatures the AFI state is retained as the glasslike arrested state when cooled in zero field. The devitrification of such a glasslike AFI state to a FMM state on a mesoscopic length scale was visualized by Wu *et al.*[8] in LPCMO single crystal. However, most of these studies (even macroscopic measurements) were focused at low temperatures. Recently, Burkhardt *et al.*[9] have shown the glassy nature of the CO-AFI state well above T_C. To directly visualize the path dependence

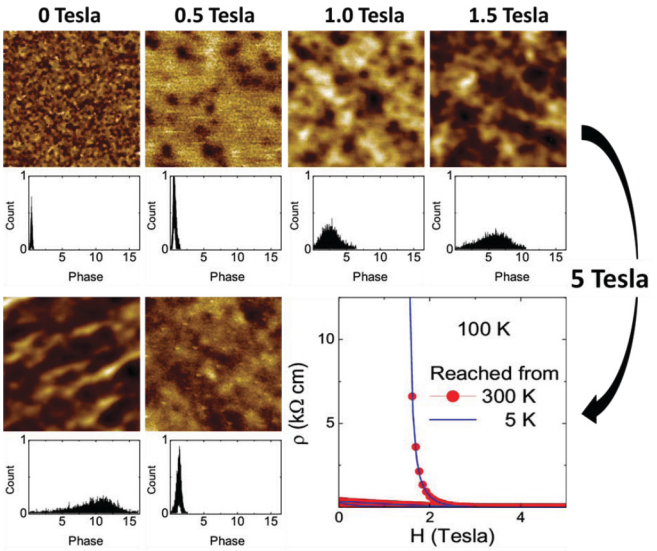

FIG. 4. (Color online) MFM images (5 μm × 5 μm) along with corresponding histograms showing magnetic field induced irreversible AFI (light region) to FMM (dark color) transition at 102 K. Bottom right panel shows an open loop in the ρ-H curves measured at 100 K after zero field cooling from 300 K (symbol) and after warming from 5 K (line).

(if any) of the AFI-FMM transition, we performed isothermal MFM and ρ-H measurements around 100 K.

Some typical MFM images along with the respective histograms at 102 K (reached by cooling in zero field) with field cycling are shown in Fig. 4. Narrow distribution of phase shift in the histogram shows a homogeneous magnetic state as observed for the $H = 0$ T image (top panel). With the application of a 0.5 T magnetic field, FMM regions with few hundreds nm size could be seen in an AFI matrix. The size of the FMM regions increases with magnetic field and by 1.5 T they form percolative paths. The distribution of phase shift above 1.5 T decreases with increasing magnetic field that is attributed to an increase in magnetic homogeneity. Relatively homogeneous MFM images at high field are not a consequence of reduced tip response, and this can be established from the images taken during field reducing cycle (from 5 T). This 0.5 T image (lower panel) has narrow distribution of phase shift, which indicates that the field induced FMM state is retained with lowering field. However, zero field image after field cycling (lower panel) shows several micrometer long regions with opposite contrast. It is similar to that observed by Zhang *et al.*[7] well below T_{MI}. The contrast in our zero field MFM image after field cycling arises due to randomly oriented domains. It is further confirmed by repeating the MFM image at 0.5 T (not shown here), which is found to be similar to that observed during the field reducing cycle at the same field value. Corresponding ρ-H behavior at 100 K (bottom right panel) also shows that the ρ remains much lower after field cycling, which was beyond measurable limit before the application of magnetic field. This figure shows the two ρ-H curves at 100 K that are measured using two different protocols; when sample temperature is stabilized at 100 K (i) after warming from 5 K (symbol) and (ii) after cooling from 300 K (line) in zero field. For both the measurement protocols, we observe

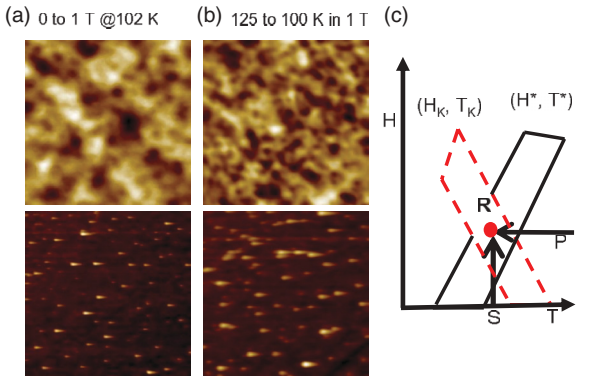

FIG. 5. (Color online) Magnetic (top panel) and topographic (bottom panel) images at 1 T (a) after zero field cooling to 102 K and (b) after field cooling to 100 K. (c) Schematic of kinetic arrest (H_K, T_K) band and supercooling (H^*, T^*) band explaining different FMM phase fraction for the two paths SR and PR.

similar behavior. In the case of first-order transition, if the measurement temperature lies within the hysteresis region of the zero field ρ-T curve, then one can obtain different states at zero field before and after field cycling. However, in that situation it would be observed either for protocol (i) or protocol (ii),[18,19] whereas the open loop due to the kinetic arrest of the first-order transition would arise for both the protocols.[18] Different zero field magnetic states before and after magnetic field cycling well below the hysteresis region of zero field ρ-T and M versus T curve have been observed in several systems[18,20–24] and have been a hallmark of CMR manganites.

Finally, we compare the nucleation and growth for the field and the temperature induced FMM state. For this we show the 1 T MFM images obtained (a) after zero field cooling (shown in Fig. 4) and (b) reached by cooling in 1 T to 100 K (shown in Fig. 2) as Figs. 5(a) and 5(b), respectively. Although the scanned regions for these two images are different (rms roughness ≈9 nm and 10 nm and topographic features ≈206 nm and 290 nm, respectively) there seems to be no correlation between topography (shown in lower panel) and respective magnetic images. Isothermal application of magnetic field at 102 K [Fig. 5(a)] results in FMM regions of larger size even though the total FMM fraction is 23%, which is much lower than that observed for the field cooled image ≈37% [Fig. 5(b)]. The difference between the two images can be explained using a phenomenological model of kinetic arrest and supercooling[14] that is shown schematically in Fig. 5(c) (for details see Kumar *et al.*[14] and Fig. 3 therein). In the absence of kinetic arrest (H_K, T_K) band, a similar FMM and AFI phase fraction is expected for these two paths. However, due to the presence of kinetic arrest (H_K, T_K) band, the AFI state is retained as a glasslike arrested state for zero field cooling. During isothermal application of magnetic field (path SR), only those AFI regions will transform into the FMM state for which respective (H_K, T_K) lines are crossed in addition to corresponding (H^*, T^*) lines. Therefore, an isothermal application of magnetic field results in a smaller FMM fraction, as some of the regions are still in AFI arrested state. From these images it can also be inferred that devitrification across the (H_K, T_K) band results in the larger size of FMM regions. This is in consonance with MFM images of Wu *et al.*,[8] which show the sudden appearance of several micron large FMM regions with increasing field as well as warming in the presence of magnetic field. They explained it as the transformation of glasslike AFI state (obtained by zero field cooling) to FMM state upon crossing the T_g [analogous to (H_K, T_K)] line.

To conclude, our MFM results directly show that the AFI-FMM transition in the LPCMO thin film cannot be explained solely in terms of broad FOPT due to quench disorder. The nucleation and growth of the FMM phase is different for the temperature and the magnetic field induced transition, and the glassy nature of the AFI state is dominant even up to 100 K. The glasslike arrested AFI state around 100 K (obtained after zero field cooling) results in larger size FMM regions with the application of magnetic field as compared to the field cooled state. During field cooling, the FMM regions grow with sub-hundred-nanometer nuclei and coalesce together with reducing temperature. The growth of the FMM region above T_{MI} gives rise to smaller ρ than expected from activated behavior.

We thank P. Chaddah for critical reading of the manuscript and many fruitful suggestions. Sachin Kumar is acknowledged for help during measurements. P.K. acknowledges CSIR, India for a Senior Research Fellowship. We thankfully acknowledge S. R. Barman for providing access to image analysis software, and Abhishek Rai and J. Nayak for helping with it.

[1] E. Dagotto, Science **309**, 257 (2005).
[2] Y. Tokura, Rep. Prog. Phys. **69**, 797 (2006).
[3] F. Macia, A. Hernandez-Minguez, G. Abril, J. M. Hernandez, A. Garcia-Santiago, J. Tejada, F. Parisi, and P. V. Santos, Phys. Rev. B **76**, 174424 (2007); F. Macia, G. Abril, A. Hernandez-Minguez, J. M. Hernandez, J. Tejada, and F. Parisi, *ibid.* **77**, 012403 (2008).
[4] L. Ghivelder and F. Parisi, Phys. Rev. B **71**, 184425 (2005).
[5] M. Uehara and S.-W. Cheong, Europhys. Lett. **52**, 674 (2000).
[6] T. Dhakal, J. Tosado, and A. Biswas, Phys. Rev. B **75**, 092404 (2007).
[7] L. Zhang, C. Israel, A. Biswas, R. L. Greene, and A. de Lozanne, Science **298**, 805 (2002).
[8] W. Wu, C. Israel, N. Hur, S. Park, S.-W. Cheong, and A. de Lozanne, Nat. Matter. **5**, 881 (2006).
[9] M. H. Burkhardt, M. A. Hossain, S. Sarkar, Y.-D. Chuang, A. G. Cruz Gonzalez, A. Doran, A. Scholl, A. T. Young, N. Tahir, Y. J. Choi, S.-W. Cheong, H. A. Dürr, and J. Stöhr, Phys. Rev. Lett. **108**, 237202 (2012).
[10] D. D. Sarma *et al.*, Phys. Rev. Lett. **93**, 097202 (2004).
[11] J. Q. He, V. V. Volkov, M. Beleggia, T. Asaka, J. Tao, M. A. Schofield, and Y. Zhu, Phys. Rev. B **81**, 094427 (2010); J. Q. He, V. V. Volkov, T. Asaka, S. Chaudhuri, R. C. Budhani, and Y. Zhu, *ibid.* **82**, 224404 (2010).
[12] V. G. Sathe, Anju Ahlawat, R. Rawat, and P. Chaddah, J. Phys.: Condens. Matter **22**, 176002 (2010).
[13] Y. Imry and M. Wortis, Phys. Rev. B **19**, 3580 (1979).

[14]K. Kumar, A. K. Pramanik, A. Banerjee, P. Chaddah, S. B. Roy, S. Park, C. L. Zhang, and S. W. Cheong, Phys. Rev. B **73**, 184435 (2006).
[15]S. B. Roy, G .K. Perkins, M. K. Chattopadhyay, A. K. Nigam, K. J. S. Sokhey, P. Chaddah, A. D. Caplin, and L. F. Cohen, Phys. Rev. Lett. **92**, 147203 (2004).
[16]H. Jeen and A. Biswas, Phys. Rev. B **83**, 064408 (2011).
[17]S. Singh, M. R. Fitzsimmons, T. Lookman, H. Jeen, A. Biswas, M. A. Roldan, and M. Varela, Phys. Rev. B **85**, 214440 (2012).
[18]P. Kushwaha, R. Rawat, and P. Chaddah, J. Phys.: Condens. Matter **20**, 022204 (2008).
[19]P. Kushwaha, A. Lakhani, R. Rawat, A. Banerjee, and P. Chaddah, Phys. Rev. B **79**, 132402 (2009).
[20]A. Banerjee, A. K. Pramanik, K. Kumar, and P. Chaddah, J. Phys.: Condens. Matter **18**, L605 (2006); A. Banerjee, K. Mukherjee, K. Kumar, P. Chaddah, Phys. Rev. B **74**, 224445 (2006).
[21]H. Kuwahara, Y. Tomioka, A. Asamitsu, Y. Moritomo, and Y. Tokura, Science **270**, 961 (1995); R. Rawat, K. Mukherjee, K. Kumar, A. Banerjee, and P. Chaddah, J. Phys.: Condens. Matter **19**, 256211 (2007).
[22]M. A. Manekar, S. Chaudhary, M. K. Chattopadhyay, K. J. Singh, S. B. Roy, and P. Chaddah, Phys. Rev. B **64**, 104416 (2001).
[23]M. K. Chattopadhyay, M. A. Manekar, A. O. Pecharsky, V. K. Pecharsky, K. A. Gschneidner, Jr., J. Moore, G. K. Perkins, Y. V. Bugoslavsky, S. B. Roy, P. Chaddah, and L. F. Cohen, Phys. Rev. B **70**, 214421 (2004).
[24]A. Lakhani, P. Kushwaha, R. Rawat, K. Kumar, A. Banerjee, and P. Chaddah, J. Phys.: Condens. Matter **22**, 032101 (2010).